

Supporting Information for:

Coarse-Grained Molecular Dynamics Simulations of Slide-ring Gels under Finite

Deformation: Influence of Sliding Ring Rearrangement on Softness and Extensibility

Contents:

- S1. Elongation rate dependence of the stress-elongation ratio curves.
- S2. Stress-relaxation behavior at several elongation ratios.
- S3. Initial configuration dependence of the stress-elongation ratio curves.
- S4. Matching of stress-extension ratio curves between simulation and experiments.
- S5. Order parameter and bond force on cross-links, axial chains and end groups.
- S6. N_{partial} distributions for all IRs.
- S7. Mooney-Rivlin plot and theoretical evaluation by Edwards-Vilgis model.
- S8. Quantitative comparison of λ_{max} defined by N_{max} and λ_c by N_0 and N_{slide}^0 .

S1. Deformation rate dependence of the stress-elongation ratio curves.

We tested two additional deformation speeds to assess the robustness of the mechanical properties of FC and SR gels with respect to the deformation rate. The original deformation rate is 100 %/10⁵τ; we also performed 100 %/10⁴τ and 100 %/10⁶τ. The resulting stress-elongation ratio curves are presented in Fig. S1(a) for FC and Fig. S1(b) for SR gels. These figures clearly show that there is only a slight dependence on deformation rate for speed below 100 %/10⁵τ. We also evaluated Young's moduli from the initial slope of the stress-elongation ratio curves and summarized in Fig. S1(c) for FC gels and S1(d) for SR gels. These graphs further indicate that the dependence of Young's moduli on the deformation rate is minimal for speeds under 100 %/10⁵τ.

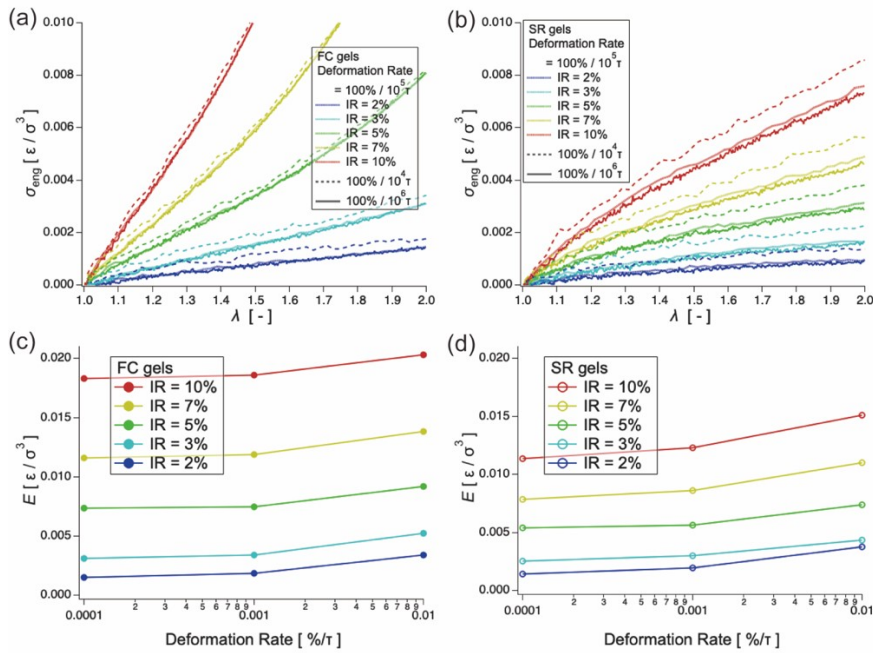


Fig. S1. Deformation rate dependence of stress-elongation ratio curves of (a)FC gels and (b)SR gels. Deformation rate dependence of evaluated Young's moduli of (c)FC gels and (d)SR gels.

S2. Stress-relaxation behavior at several elongation ratios.

To assess mechanical equilibrium, we extracted stress-relaxation curve from snapshots taken during the equilibration calculation just after elongation at $\lambda = 1, 2, 3, 4$, and 5. The obtained stress-relaxation curve is shown in the Fig. S2. From the figure, almost no mechanical relaxation is observed. Additionally, as demonstrated in Fig. S1., the stress-elongation curves exhibit only slight dependence on the stretching speed around $100\%/10^5\tau$. Thus, we conclude that the uniaxial elongation is conducted under quasi-stable conditions.

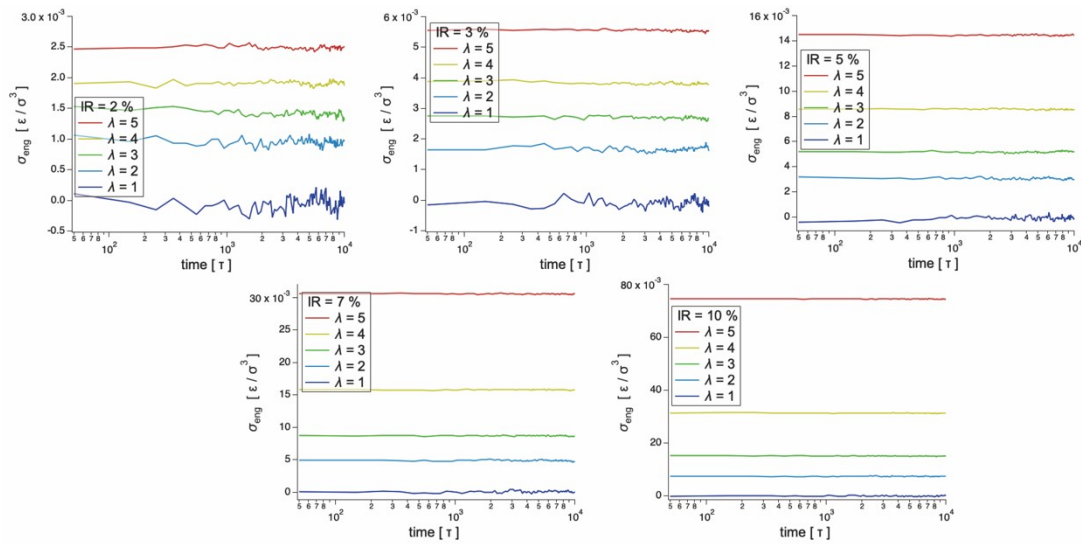


Fig. S2. Stress relaxation during equilibration calculation with several elongation ratios

For further information, the sliding diffusion coefficient of the ring along the chain is $D_{\text{slide}} = 0.132 \sigma^2/\tau$,¹ then time required for a ring to slide along the average partial chain length (N_0^{exp}) is

defined as the characteristic sliding time $\tau_{\text{slide}} \approx (N_0^{\text{exp}})^2 / 2D$ and calculated as following Table

S1:

Table. S1. Characteristic sliding time (τ_{slide})

IR [%]	2	3	5	7	10
τ_{slide} [τ]	1.2×10^4	5.3×10^3	1.9×10^3	1.0×10^3	5.3×10^2

It is evident that τ_{slide} is much shorter than the time required for 100% deformation ($10^5\tau$), then

we considered the systems are well-equilibrated.

S3. Initial configuration dependence of the stress-elongation ratio curves.

The main results are based on elongation along z-direction. To assess the influence of initial configuration on the stress-elongation ratio curves, we also conducted elongation simulations along the x and y directions. Additionally, we fabricated alternative configuration for all inclusion ratios (IRs) using the procedure described in the main text. The binding ratio and cross-linking density for these the additional samples are presented in Table S2., which shows that the additional configuration exhibits cross-linking densities similar to those of original samples. Using both the original and the additional configurations, we obtained stress-elongation ratio curves for three directions (6 samples per IR) and the results are summarized in Fig. S3. In this figure, the stress-elongation ratio curves discussed in the main text is shown in solid lines, and the those for two other elongation directions are depicted as broken lines. The curves for the additional configuration are illustrated as dotted lines. Overall, the figure demonstrated that the initial configuration has only a slight effect on stress-elongation ratio curves is slight for both FC and SR gels.

Table S2. Inclusion ratio (IR), binding ratio (r_B) and cross-linking density (ν_C) for additional configuration

Sample	IR 2%	IR 3%	IR 5%	IR 7%	IR 10%
IR [%]	2	3	5	7	10
r_B [%]	87.8	91.1	85.8	86.3	82.2
ν_C [$10^{-3}\sigma^{-3}$]	0.70	1.09	1.71	2.42	3.29

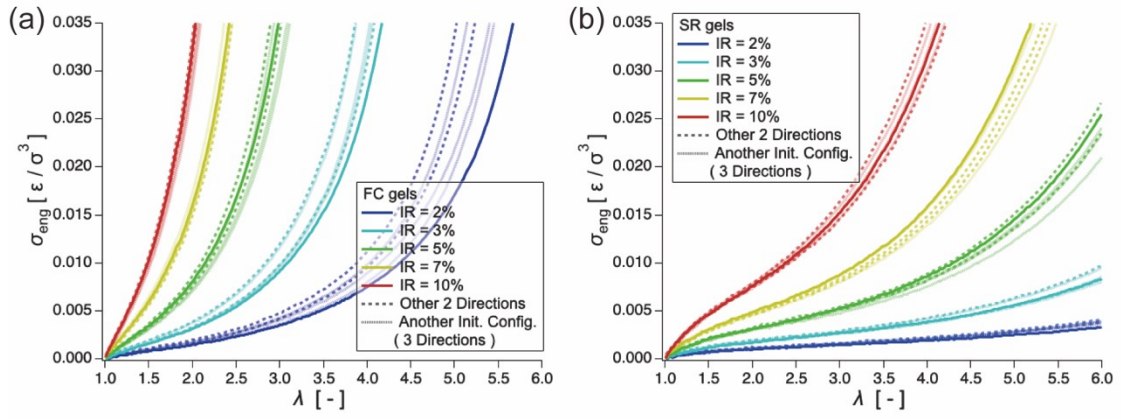


Fig. S3. Initial configuration, stretching direction dependence of the stress-elongation ratio curves with (a) FC and (b)SR gels.

S4. Matching of stress-extension ratio curves between simulation and experiments.

For IR=2%, we compared the simulated stress-elongation ratio curve to experimental ones².

Fig. S4 shows the comparison, and the simulated curve reproduced the stress-softening behavior against Neo-Hookean model.

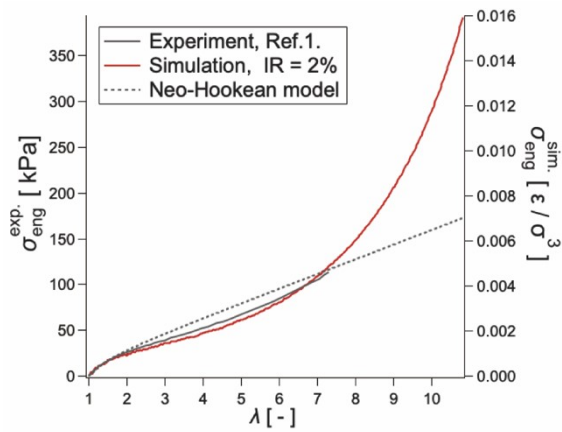


Fig. S4. Comparison of stress-extension ratio between curve obtained from experiment (left axis, ref. 1.) and that obtained from the simulation (right axis, IR = 2%).

S5. Order parameter and bond force on cross-links, axial chains and end groups.

In the main text, we only show the order parameters and average forces on the axial chains.

Here we present the composition of kinetic energy, nonbonded potential, angle potential, and

bonded potential relative to total energy as shown in Fig. S5. In Fig. S5(a), it is clear that the

bonded potential is the dominant component of the total energy, independent of the elongation

ratio. From S5(b) shows the deviation against undeformed state($\lambda=1$), defined as $\Delta U_{\text{angle}}(\lambda)$ and

$\Delta U_{\text{bond}}(\lambda)$. The figure indicates that $\Delta U_{\text{angle}}(\lambda)$ are much smaller than $\Delta U_{\text{bond}}(\lambda)$.

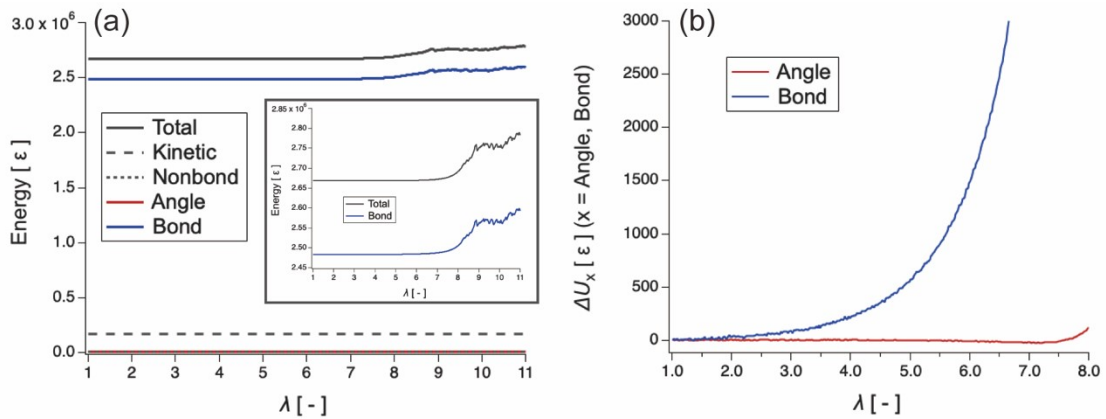


Fig. S5. (a) Total energy, kinetic energy, nonbonded potential, angle potential, and bonded

potentials as a function of elongation ratio. The inset figure shows a zoomed view highlighting

that the main component of the energy is the bonded potential. (b) the deviation of angle and

bonded potential against undeformed state($\lambda=1$), denoted as ΔU_{angle} , and ΔU_{bond} , respectively.

We also classified the bonds into cross-linking bonds and end bonds as defined as Figure S6(a), and the order parameters of and average forces loaded on these bonds are plotted against elongation ratio in Figures S6 (b-e). As shown in Fig. S6 (b) and S6 (c), end bonds in both FC and SR gel orient less to stretching direction, while both cross-links (CLs) and axial bonds orient to stretching direction for both FC and SR gels. Cross-links for SR gels orient weaker than axial chain, suggesting that part of cross-linking bonds orient perpendicular to the stretching direction as illustrated in Figure S6 (f). For stress load shown in Figures S6 (d) and (e), FC gel shows similar tendency, stress are loaded on both axial chains and cross-links, no stress is loaded on ends, and SR gels shows that similar stress are loaded on axial chains and end bonds, which is consistent with the fracture mechanisms suggested by Uehara et al³. It shows that network strands stretched out for rings to reach ends, as illustrated in Figure S6 (f).

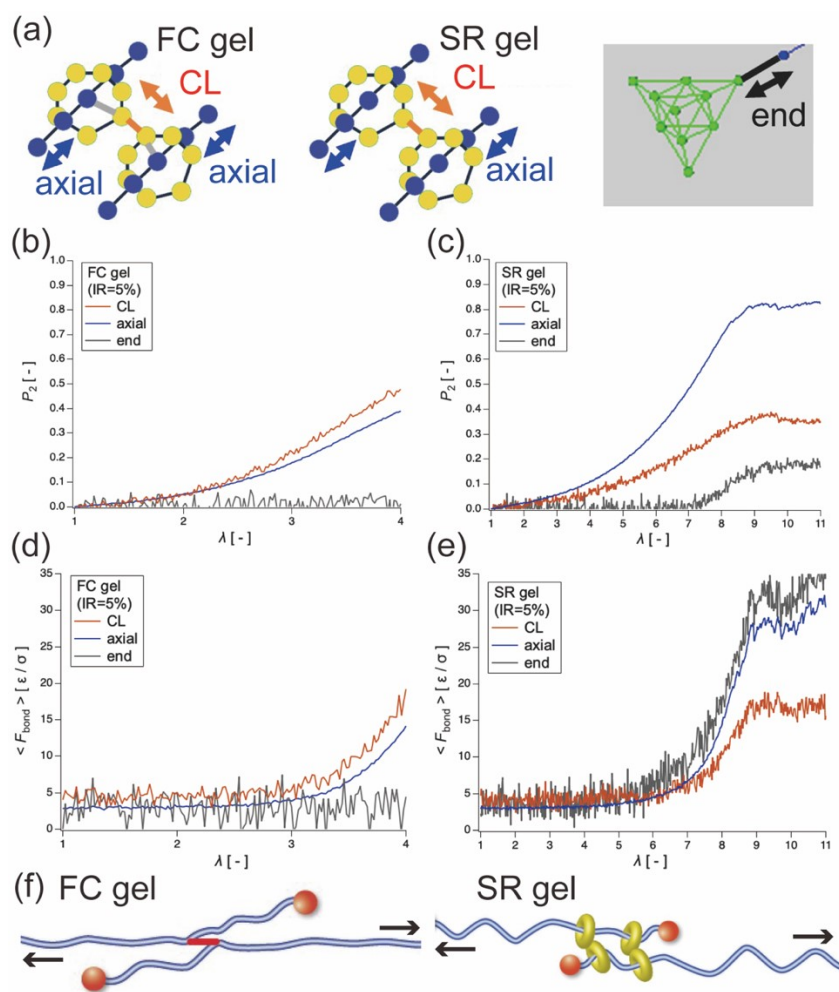


Fig. S6. (a) Schematic illustrations of CL, axial and end bond. (b,c) Order parameters of each bond in (b)FC and (c)SR gels under deformation. (d,e) Average force loaded of each bond in (d)FC and (e)SR gels under deformation. (f) Schematic illustrations of suggested mechanism.

S6. N_{partial} distributions for all IRs.

In the main text, we showed network strand length distribution change against elongation ratio and analyzed N_0 , N_{max} , N_{slide} by bimodal exponential function for sample of IR = 5 %. For confirmation of the argument in the main text, we also conducted the analysis in the similar way for IR = 2,3,7, and 10 % as shown in Fig. S7.

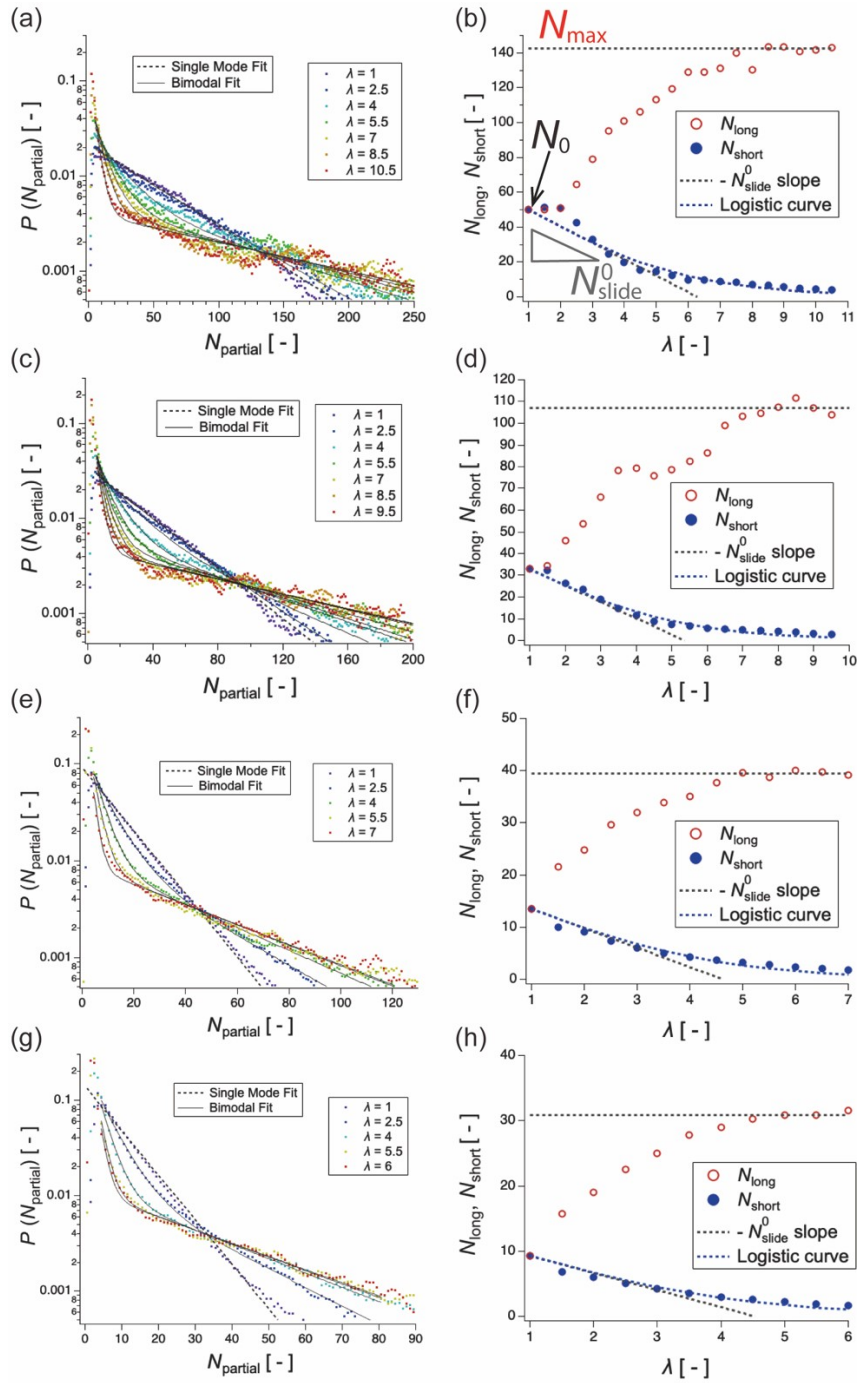


Fig. S7. (a,c,e,g) Distribution of N_{partial} , for SR gel with (IR = (a)2%, (c)3%, (e)7%, (g)10%). The dotted line is the fitting result by the single exponential fit (Eq. 13) for $\lambda = 1$, and the solid lines are the fitting lines by the bimodal function (Eq. 15). (b,d,f,h) λ dependence of N_{short} and N_{long} for SR gel with IR = (b)2%, (d)3%, (f)7%, (h)10%).

S7. Mooney-Rivlin plot and theoretical evaluation by Edwards-Vilgis model.

As described in the main text, there is a similarity in our sliding parameter N_{slide}^0/N_0 and the slipping parameter η in the Edwards-Vilgis model.^{4,5} We begin with the free energy in the Edwards-Vilgis model without inextensibility ($\alpha \rightarrow 0$ limit of Eq. 4.32, which is equivalent to Eq. 2.14 in their literature^{4,5}).

$$F = \frac{1}{2}N_c \sum_{i=1}^3 \lambda_i^2 + \frac{1}{2}N_s \sum_{i=1}^3 \left\{ \frac{\lambda_i^2(1+\eta)}{1+\eta\lambda_i^2} + \log(1+\eta\lambda_i^2) \right\} \quad (S1)$$

Where N_c and N_s is the numbers of fixed cross-links and slip-links in the system. Under uniaxial elongation, the engineering stress (σ_{eng}) -elongation ratio (λ) relationship is given by:

$$\sigma_{eng} = \frac{N_c}{V} \left(\lambda - \frac{1}{\lambda^2} \right) + \frac{N_s}{V} \left[(1+\eta) \left\{ \frac{\lambda}{(1+\eta\lambda^2)^2} - \frac{1}{(\lambda+\eta)^2} \right\} + \eta \frac{\lambda \left(\lambda - \frac{1}{\lambda^2} \right)}{(1+\eta\lambda^2)(\lambda+\eta)} \right] \quad (S2)$$

Where V is the volume of the system. The reduced stress ($\sigma_{eng}/(\lambda+\lambda^{-2})$) is expressed as:

$$\frac{\sigma_{eng}}{\lambda - \frac{1}{\lambda^2}} = \frac{N_c}{V} + \frac{N_s}{V} \left[(1+\eta) \frac{\lambda^2(1-\eta^2\lambda)}{(1+\eta\lambda^2)^2(\lambda+\eta)^2} + \eta \frac{\lambda}{(1+\eta\lambda^2)(\lambda+\eta)} \right] \quad (S3)$$

If only slip-links present in the system ($N_c = 0$), the $\lambda \rightarrow 1$ limit (i.e. shear modulus) and the initial slope of the reduced stress are given by:

$$G_s = \left. \frac{\sigma_{eng}}{\lambda - \frac{1}{\lambda^2}} \right|_{\lambda=1} = \frac{N_s/V}{(1+\eta)^2} \quad (S4)$$

$$\left. \frac{\partial}{\partial \lambda^{-1}} \left(\frac{\sigma_{eng}}{\lambda - \frac{1}{\lambda^2}} \right) \right|_{\lambda=1} = \frac{N_s}{V} \frac{2\eta}{(1+\eta)^3} \quad (S5)$$

Conversely, if only fixed cross-links are present ($N_s = 0$), the $\lambda \rightarrow 1$ limit of the reduced stress is

$$G_c = \left. \frac{\sigma_{eng}}{\lambda - \frac{1}{\lambda^2}} \right|_{\lambda=1} = \frac{N_c}{V} \quad (S6)$$

Thus, the ratio of the moduli for the slip-link model to non-slip model is:

$$\left. \frac{G_s}{G_c} \right|_{N_s = N_c} = \frac{1}{(1+\eta)^2} \quad (S7)$$

Using affine network model as non-slip model, we have

$$G_s = \left. \frac{\sigma_{eng}}{\lambda - \frac{1}{\lambda^2}} \right|_{\lambda=1} = \frac{G_{affine}}{(1+\eta)^2} \quad (S8)$$

$$\left. \frac{\partial}{\partial \lambda^{-1}} \left(\frac{\sigma_{eng}}{\lambda - \frac{1}{\lambda^2}} \right) \right|_{\lambda=1} = G_{affine} \frac{2\eta}{(1+\eta)^3} \quad (S9)$$

We construct a model for reduced stress ($\sigma_{eng}/(\lambda+\lambda^{-2})$) – inverse elongation ratio (λ^{-1}) curve using

substitution $\eta = N_{slide}^0 / N_0$

$$\frac{\sigma_{eng}}{\lambda - \frac{1}{\lambda^2}} = \frac{G_{affine}}{\left(1 + \frac{N_{slide}^0}{N_0}\right)^2} + G_{affine} \frac{2 \frac{N_{slide}^0}{N_0}}{\left(1 + \frac{N_{slide}^0}{N_0}\right)^3} (\lambda^{-1} - 1) \quad (S10)$$

These model curves are plotted alongside the Mooney-Rivlin plots from the uniaxial elongation

simulation in Fig. S8(a). The graph shows that slope near the initial elongation ($1/\lambda \sim 1$) closely matches that of the model (Eq. S10). In contrast, the Mooney-Rivlin plots for FC gels exhibit almost no decay (Fig. S8 (b)). Hence, we conclude that slipping parameter η corresponds to N_{slide}^0 / N_0 in our SR gels.

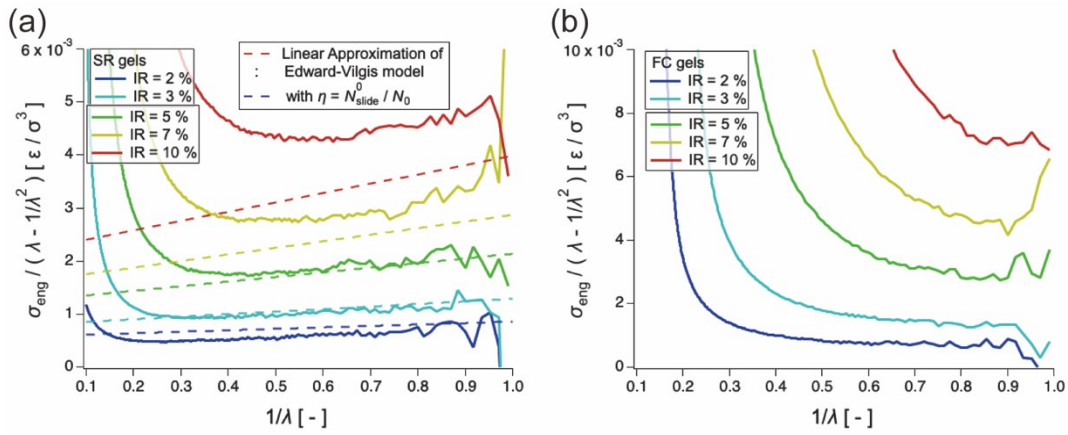


Fig. S8. Mooney-Rivlin plot of (a)SR gels and (b)FC gels obtained from mechanical simulation with model estimation by Equation S10.

For further information, we also calculated the number of topological kinks per chain, $\langle Z \rangle$, from the last $2 \times 10^5 \tau$ snapshots in the initial $1 \times 10^6 \tau$ relaxation calculation of the entire system using Z1+ code.⁶ The values of $\langle Z \rangle$ and number of rings pre chain are summarized in Table S3. The table indicates that there are only a few entanglements between axial chains, which corresponds to the result that the Mooney-Rivlin plots for FC gels show almost no decay (see Fig. S8(b)).

Table S3. the comparison of $\langle Z \rangle$ and the number of rings per chain.

IR [%]	2	3	5	7	10
$\langle Z \rangle$	1.44	1.61	1.725	1.93	2.22
Num. rings	8	12	20	28	40

S8. Quantitative comparison of λ_{\max} defined by N_{\max} and λ_c by N_0 and N_{slide}^0 .

In the main text, we defined λ_{\max} based on the value of N_{\max} . In this section, we define the critical elongation ratio λ_c as $\lambda_c = N_0 / N_{\text{slide}}^0$, which corresponds to the elongation ratio at which N_{short} reaches zero. As shown in the Table S4 below, λ_{\max} and λ_c have similar values. This indicated that finite extensibility appears when N_{short} becomes zero, corresponding to the stacking of the neighboring two figure-of-eight cross-links. And at the same time, the longer chains reach the maximum chain length N_{\max} , and are fully extended.

Table S4. Quantitative comparison of λ_{\max} and λ_c

IR [%]	2	3	5	7	10
λ_{\max}	8.64	7.50	5.51	4.56	4.03
λ_c	6.29	5.36	4.89	4.62	4.53

References

- 1 Y. Yasuda, M. Toda, K. Mayumi, H. Yokoyama, H. Morita and K. Ito, Sliding Dynamics of Ring on Polymer in Rotaxane: A Coarse-Grained Molecular Dynamics Simulation Study, *Macromolecules*, 2019, **52**, 3787–3793.
- 2 C. Liu, K. Mayumi, K. Hayashi, L. Jiang, H. Yokoyama and K. Ito, Direct Observation of Large Deformation and Fracture Behavior at the Crack Tip of Slide-Ring Gel, *J. Electrochem. Soc.*, 2019, **166**, B3143–B3147.
- 3 S. Uehara, Y. Wang, Y. Ootani, N. Ozawa and M. Kubo, Molecular-Level Elucidation of a Fracture Process in Slide-Ring Gels via Coarse-Grained Molecular Dynamics Simulations, *Macromolecules*, 2022, **55**, 1946–1956.
- 4 R. C. Ball, M. Doi, S. F. Edwards and M. Warner, Elasticity of entangled networks, *Polymer*, 1981, **22**, 1010–1018.
- 5 S. F. Edwards and Th. Vilgis, The effect of entanglements in rubber elasticity, *Polymer*, 1986, **27**, 483–492.
- 6 M. Kröger, J. D. Dietz, R. S. Hoy and C. Luap, The Z1+ package: Shortest multiple disconnected path for the analysis of entanglements in macromolecular systems, *Computer Physics Communications*, 2023, **283**, 108567.